Clays and Clay Minerals, Vol. 54, No. 5, 598–604, 2006.

DISSOLUTION OF BRUCITE ON THE (001) SURFACE AT NEUTRAL pH: *IN SITU* ATOMIC FORCE MICROSCOPY OBSERVATIONS

YURIKO KUDOH, JUN KAMEDA AND TOSHIHIRO KOGURE*

Department of Earth and Planetary Science, Graduate School of Science, The University of Tokyo, 7-3-1 Hongo, Bunkyo-ku, Tokyo, 113-0033, Japan

Abstract—The dissolution of brucite, $Mg(OH)_2$, on the (001) surface was investigated using *in situ* atomic force microscopy in solutions at near-neutral pH. Dissolution proceeded by the formation of crystallographically oriented triangular etch pits with monolayer step and expansion of the pits. The sides of the triangle are parallel to the [100], [110] and [010] directions of the brucite structure, and the orientation of lines from the center of the triangle to the three apices are along the [210], [$\bar{1}$10] and [$\bar{1}\bar{2}$0] directions. This orientation may produce pit edges where OH groups coordinate to two Mg^{2+}. Although triangular etch pits with monolayer depth formed mostly at random on the (001) surface, concentric pits penetrating several layers were also observed. Etch pits with spiral steps were rarely observed. Coalescence of the pits resulted in stranded terraces that diminished in size rapidly and formed a rounded irregular form. The step-retreat velocity around the triangular pit is 0.015−0.04 nm/s at pH 5−8. The retreat velocity around the stranded terraces was about three times more rapid than that around the triangular etch pits.

Key Words—Atomic Force Microscopy, Brucite, Dissolution, Etch Pit, Step Velocity.

INTRODUCTION

Because of the importance of the dissolution of minerals in the weathering cycle, numerous experimental studies have been conducted to determine the dissolution rates of minerals at various conditions, mainly by reaction experiments of powdered minerals and solutions. Results of these studies were summarized, for example, by White and Brantley (1995). Scanning probe microscopy, especially atomic force microscopy (AFM) that can image the surface topography of insulating materials in various environments (Binning *et al*., 1986), has provided a new method of investigating dissolution phenomena of solid materials. Microscopic imaging at the atomic scale and *in situ* observation of the dissolution process has given an understanding of atomistic dissolution mechanisms on mineral surfaces (*e.g*. Bosbach and Rammensee, 1994; Heaton and Engstrom, 1994; Dove and Platt, 1996; Shiraki *et al*., 2000).

Brucite, $Mg(OH)_2$, is a layered hydroxide mineral occurring as a precipitate from basic solutions. Although the natural occurrence of brucite is not so frequent, brucite is considered an important mineral for study because its structure is a basic unit of other layered minerals, such as chlorite and hydrotalcite. The dissolution behavior of brucite seems essential to understand the dissolution processes of other layered minerals. Brucite is also a practical material to investigate by AFM owing to its relatively rapid dissolution rate suitable for study in real time and because it has perfect (001) cleavage.

Vermilyea (1969) investigated the dissolution rate and its pH dependence of synthetic and natural brucite, by dissolving powder in solution and monitoring the pH of the solution. He also reported that the dissolution slowed considerably for 'aged' specimens (portions remaining after the first dissolution experiment). Recently, Pokrovsky and Schott (2004) investigated the dissolution rate of brucite and its dependence on pH, ionic strength and saturation index. In their study, the dissolution rate decreased more gradually as pH increased than that reported by Vermilyea (1969). They also reported the effect of various organic and inorganic ligands, and divalent metal ions on the dissolution rate (Pokrovsky *et al*., 2005). In addition to these 'bulk' dissolution experiments, Jordan and Rammensee (1996) studied the dissolution of brucite in nitric acid at pH 2.73 by using AFM. They found that the dissolution of brucite on the (001) surface proceeds by the retreat of monolayer steps. They determined the dissolution rate from the step-retreat velocity, and calculated the activation energy of dissolution by varying reaction temperatures. They also observed that the step-retreat velocity is dependent on step density or the length of the terraces between steps; this suggested the importance of interstep interaction for the dissolution of brucite. Dissolution processes of related materials, periclase (MgO) and gibbsite ($Al(OH)_3$), were also investigated using AFM (Jordan *et al*., 1999; Peskleway *et al*., 2003).

* E-mail address of corresponding author:
kogure@eps.s.u-tokyo.ac.jp
DOI: 10.1346/CCMN.2006.0540506

Copyright © 2006, The Clay Minerals Society

https://doi.org/10.1346/CCMN.2006.0540506 Published online by Cambridge University Press

The present paper describes the dissolution features of brucite at near-neutral pH using *in situ* AFM that incorporates a fluid cell. Probably owing to the difference of pH, the dissolution feature observed here is considerably different from that described by Jordan and Rammensee (1996). The purpose of the study is to understand the dissolution process of brucite at near-neutral pH, rather than to determine the absolute dissolution rate of the mineral.

EXPERIMENTAL

The brucite specimen studied was a colorless, large crystal from Wood's mine, Pennsylvania, USA. Electron-probe microanalysis detected no impurity elements within detection error. Thin crystals of ~0.1 cm^2 in area were fixed with epoxy resin on steel plates and then carefully cleaved in air using Scotch-brand tape just prior to immersion in solutions.

The AFM imaging was performed using a Digital Instruments NanoScope IIIa. Surface images were acquired in contact mode using 200 μm long Si_3N_4 cantilevers with 0.12 N/m spring constant. The loading force applied was between 30 and 80 nN. To avoid damage to the surface by the scanning of the cantilever, the AFM images were obtained every 100 s. A Digital Instruments fluid cell was used. The volume of the solution in the cell was 0.5 cm^3. To avoid perturbation involving fluid flow and to acquire clear images, a flow-through system was not used. A standard solution of potassium hydrogen phthalate (0.05 mol/L, pH 4.0) for the calibration of pH meters (Horiba, Ltd., Japan) was used for the solution at pH 4. This solution was diluted with de-ionized water by ~1500 times to obtain pH 5 solution. The basic solutions (pH 8 and 9.2) were similarly prepared using a standard solution from Horiba, Ltd. of sodium tetraborate (0.01 mol/L, pH 9.2) and the standard solution was also diluted about 1500 times for pH 8. For the dissolution experiments, de-ionized water was also used. An increase of pH may have occurred during the experiment, owing to the dissolution of brucite and the static solution system. Hence the reported pH of the solutions is for the initial stage (any change of pH during the experiment is discussed below). The temperature for the dissolution experiment was kept constant at 22−25ºC. The crystal orientation of the brucite specimen was determined by the electron back-scattered diffraction (EBSD) technique using a PhaseID system (ThermoNoran Inc.) on an Hitachi S-4500 scanning electron microscope (SEM) (Kogure, 2002).

RESULTS AND DISCUSSION

Dissolution feature on the (001) surface

Figure 1a shows a typical surface image of the (001) surface at pH 5 with respect to time. Each AFM image is produced by the differential of height and steps observed in the image have a height of 0.5 nm. This height corresponds to a single $Mg(OH)_2$ layer of brucite. Immediately after immersion, the (001) terraces were coarse, but they became atomically smooth after ~10 min as dissolution proceeded. From Figure 1a, the dissolution of brucite is shown to proceed by the formation of triangular etch pits followed by expansion of the pits laterally. The equilateral triangular shape is expected because the crystal structure of brucite has a three-fold ($\bar{3}$) axis normal to the (001) surface. The etch pits coalesce as they expand and form stranded terraces on the surface (white arrow in Figure 1a). Early in the process, stranded terraces possess a triangular shape with a reverse orientation to that of the etch pits. Then the terraces evolve to a rounded shape by rapid dissolution near the apices. The step density is roughly constant with the generation of new pits, expansion and coalescence of the pits, and diminution of the stranded terraces (Figure 1b). Although most etch pits with a monolayer depth form randomly on the flat surface (Figure 1a), concentric triangular pits are occasionally observed (Figure 2a). The latter observation suggests that the origin (probably some structural defect) of the etch pits penetrates several layers. Etch pits with spiral steps (Figure 2b) were also observed, implying a screw dislocation. However, their occurrence was rare.

The dissolution feature was similar in the solutions at pH 5 and 8, and in de-ionized water. In contrast, dissolution was rapid and the resultant surface topography was unique at pH 4 (Figure 3). At this pH, large and deep trigonal etch pits formed. The slope of the sides of the pit has an inclination angle of 1º and the slope consists of a high density of monolayer steps (Figure 3b). Jordan and Rammensee (1996) reported the formation of triangular etch pits in their AFM observation, but they did not present images suitable for comparison to Figure 3 in which each etch pit is large and deep, and the step density on the slopes around the pits is high. The origin of these deep etch pits is probably the same as those in Figure 2; they are probably related to dislocations intersecting the surface. The difference in surface topographies between Figures 2 and 3 may be related to the rapid dissolution along the dislocation core in the acidic solution. The surface topography did not change at pH 9.2, owing to a very slow dissolution rate.

The relationship between etch pit geometry and crystallography

To determine the relationship between the triangular etch pits and the crystal structure of brucite, the remaining crystal was coated with amorphous carbon for EBSD analysis in the SEM. Figure 4a shows an EBSD pattern obtained from the surface and Figure 4b represents the AFM image of the surface. The sides of the triangle are parallel to the [100], [110] and [010] directions, and the directions from the center of the

https://doi.org/10.1346/CCMN.2006.0540506 Published online by Cambridge University Press

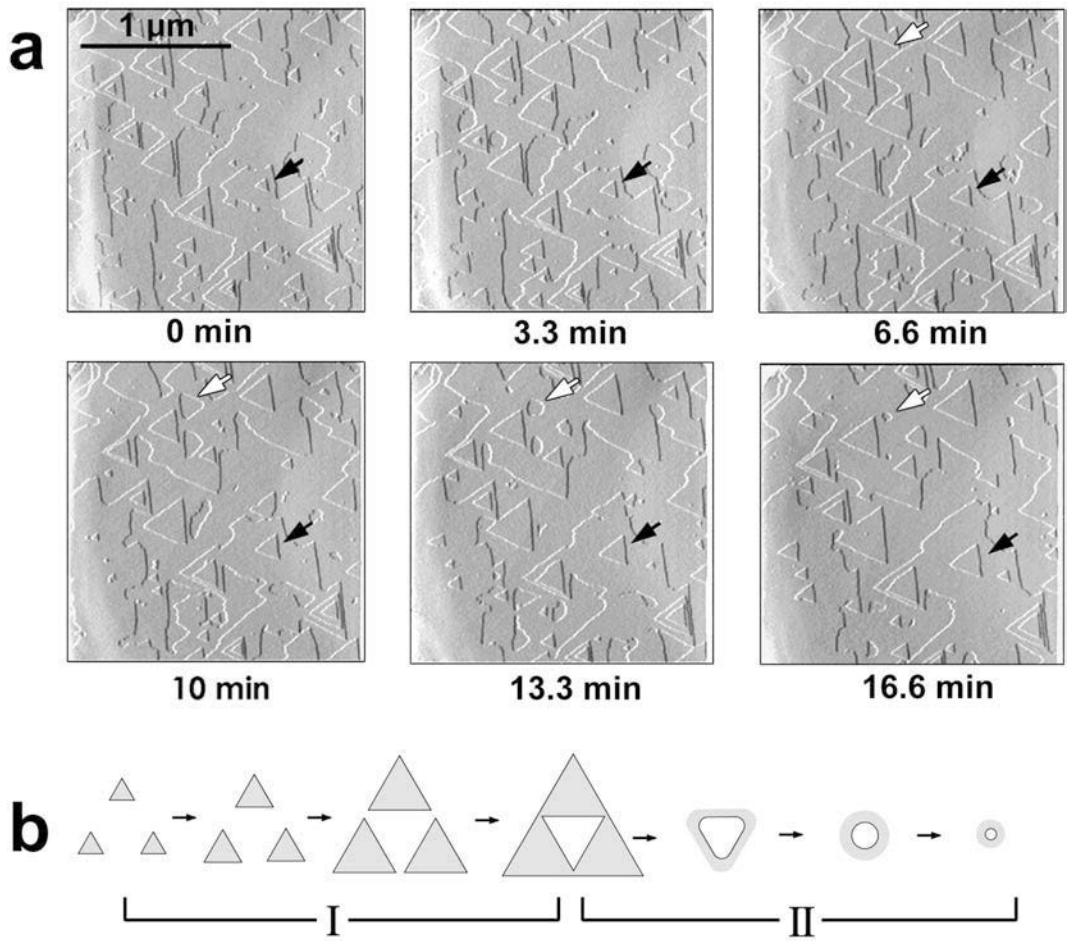


Figure 1. (a) AFM images showing the surface microtopography of brucite in solution at pH 5. These images and those in the other figures are expressed by differential mode. The step height is 0.5 nm and this height corresponds to the monolayer thickness of $Mg(OH)_2$. The black arrow indicates the same triangular etch pit in each image, expanding in size with time. The white arrow shows a stranded terrace formed by the coalescence of etch pits, diminishing in size with time. (b) A diagram to show the dissolution process of brucite on the (001) surface. Triangular etch pits form and expand until they coalesce (I). A stranded terrace forms by the coalescence of the pits and diminishes in size with a rounded shape (II).

triangle to the apices are [210], [$\bar{1}$10] and [$\bar{1}\bar{2}$0]. A structure model of the etch pit is proposed in Figure 4c. In the brucite structure, one hydroxyl (OH) group coordinates to three Mg^{2+} ions and the O-H vector is perpendicular to the (001) plane. The H atom forms hydrogen bonds to three oxygen atoms on the adjacent brucite sheet. Based on this model (Figure 4c), one OH group coordinates to two Mg^{2+} along the edge of the surface (upper) OH plane and one OH group coordinates to one Mg^{2+} along the edge of the lower OH plane. If the triangle of the pit is rotated by 60º or 180º, then the OH groups coordinating to one Mg^{2+} align on the surface edge. Although a rigorous energy calculation including hydrogen bonding with the lower brucite sheet is required, it is likely that the edge structure in Figure 4c where the surface OH groups coordinate to two Mg^{2+} is more stable than that with OH groups coordinating to one Mg^{2+} along the surface edge.

Determination of step-retreat velocity and estimation of the dissolution rate

In solutions at near neutral pH, the dissolution of brucite on the (001) surface progresses by expansion of triangular etch pits and by extinction of stranded terraces. The dissolution rate (R) on the (001) surface is given by:

$$R = vlc/V\mathrm{N}_A \ (\mathrm{mol/m^2/s}) \qquad (1)$$

where v, l, c, V and $\mathrm{N_A}$ express the retreat velocity of the step, step density (total length of the steps per unit surface area), step height (equal to the c axis), the volume of a molecule that is equal to the cell volume of brucite because Z (formula units per cell) is equal to one, and Avogadro's number, respectively. In general, estimation of the step velocity (v) from sequential AFM images is difficult owing to drift of the specimen during observation. However, the step velocity around the etch pits can

https://doi.org/10.1346/CCMN.2006.0540506 Published online by Cambridge University Press

be estimated from the area (S) of the triangular etch pit until neighbors contact each other. If we denote x as the distance from the center of the triangle to its side, then the step retreat velocity (v) around the etch pits is given by:

$$v = \mathrm{d}x/\mathrm{d}t \quad (2)$$

By geometry, S is related to x as (Figure 5a):

$$S = 3\sqrt{3}x^2 \quad (3)$$

The areas of the triangular etch pits were measured in AFM images and x was calculated using equation 3. In Figure 5a, x is plotted as a function of time for three etch-pits in Figure 1a (pH 5). The slope of the lines (step velocity) is nearly constant and independent of time. The step velocity around the stranded terraces was similarly calculated from the area of the terraces. In this case, the terrace was approximated as a circle and step velocity was calculated from the change of the radius with time (Figure 5b). The step velocity around the stranded terraces is about three times greater than the step velocity around the triangular etch pits. The difference in step velocity is probably related to the atomic arrangement at the straight steps around the triangular pits (Figure 4c) which is more stable than the arrangement around the stranded terraces.

Figure 5c shows the step velocity as a function of pH around the triangular pits. The velocity at pH 5 is the greatest. Step density (l) is required to calculate the dissolution rate from equation 1. For instance, the step density in the bottom-right image of Figure 1a is 0.0077 nm^{-1}, which was obtained by measuring the total length of the step in the image and dividing it by the image area. Assuming that the length of the steps around the triangular pits is equal to that of the steps around the stranded terraces, the dissolution rate is calculated to be 1.0×10^{-8} mol m^{-2} s^{-1} at pH 5 and 5.0×10^{-9} mol $m^{-2}s^{-1}$ at pH 8. These values are 20% of those reported by Pokrovsky and Schott (2004), which were derived from the bulk dissolution experiment. This discrepancy is reasonable, considering the different experimental methods used. However, the accuracy of the above values needs to be considered.

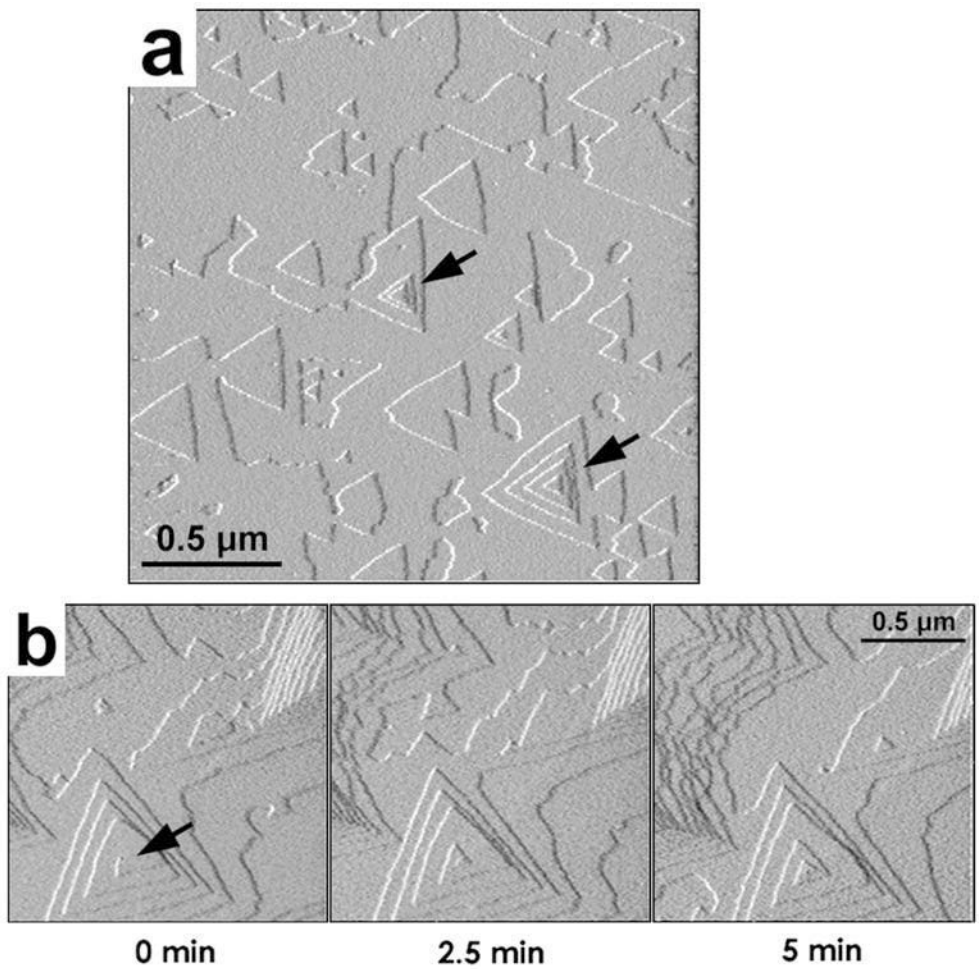


Figure 2. (a) Concentric triangular etch pits (arrow) developed during dissolution. (b) An etch pit with spiral steps.

https://doi.org/10.1346/CCMN.2006.0540506 Published online by Cambridge University Press

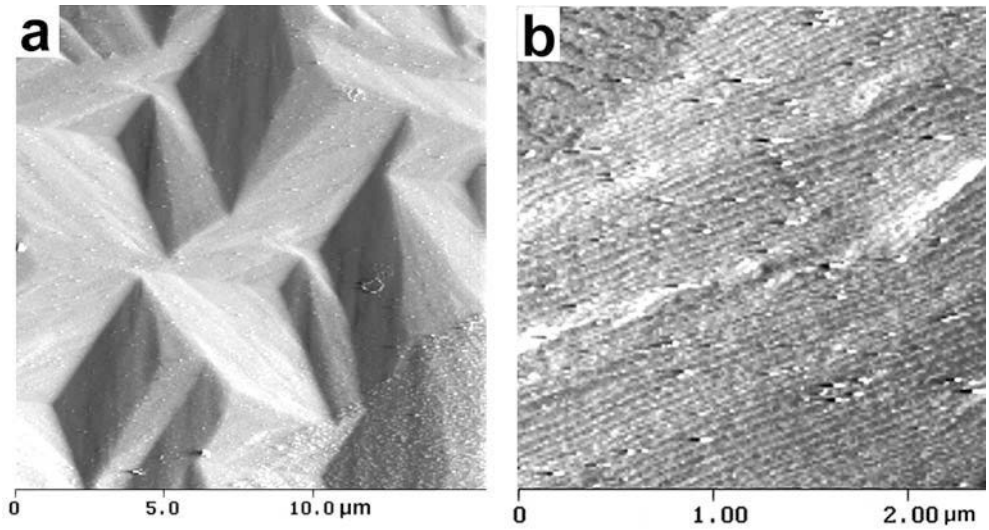


Figure 3. Microtopography of the (001) surface developed during the dissolution at pH 4. (a) Low magnification AFM image. (b) Higher magnified image showing the 0.5 nm steps on the slope. The inclination of the slope is ~1°.

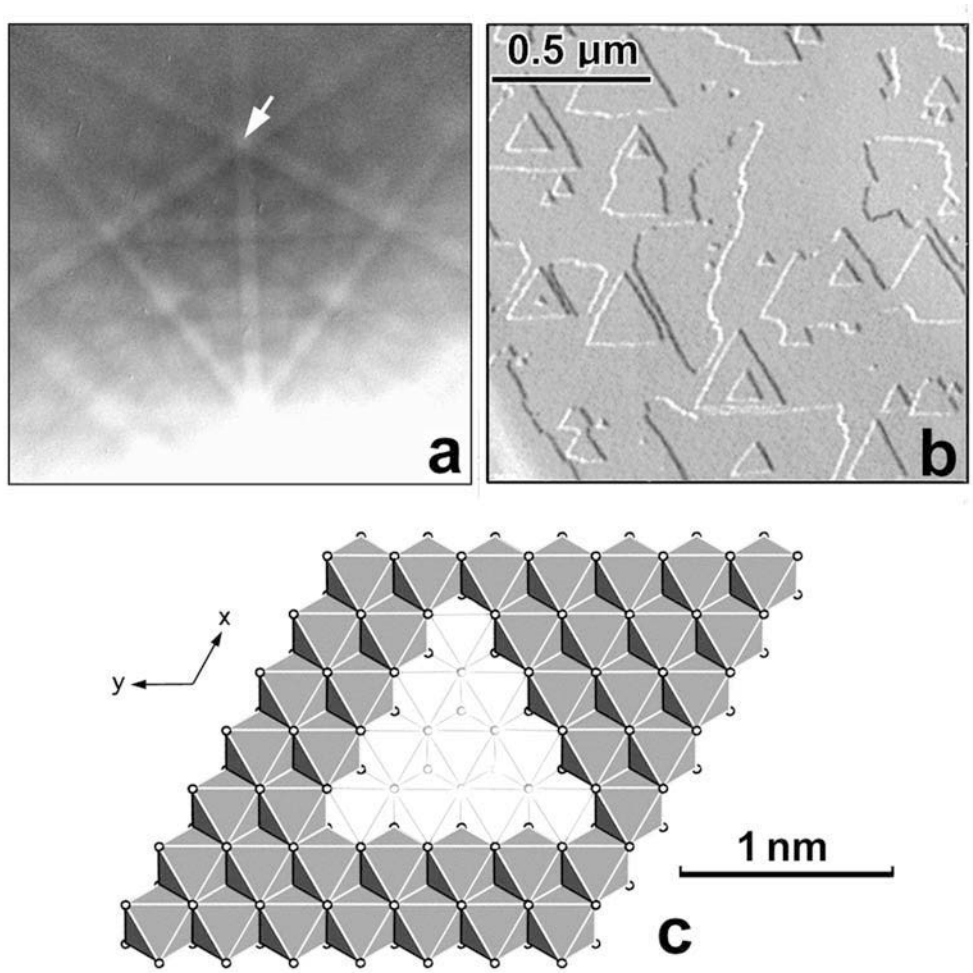


Figure 4. (a) EBSD pattern from the (001) surface after the dissolution experiment in the AFM fluid cell. The white arrow indicates the direction normal to the substrate (the [001] direction), showing the three-fold symmetry. (b) AFM image from the surface with the same orientation as that in (a). (c) Structure model of the triangular etch pit proposed from the relationship between the surface topography by AFM and crystal orientation determined by EBSD.

https://doi.org/10.1346/CCMN.2006.0540506 Published online by Cambridge University Press

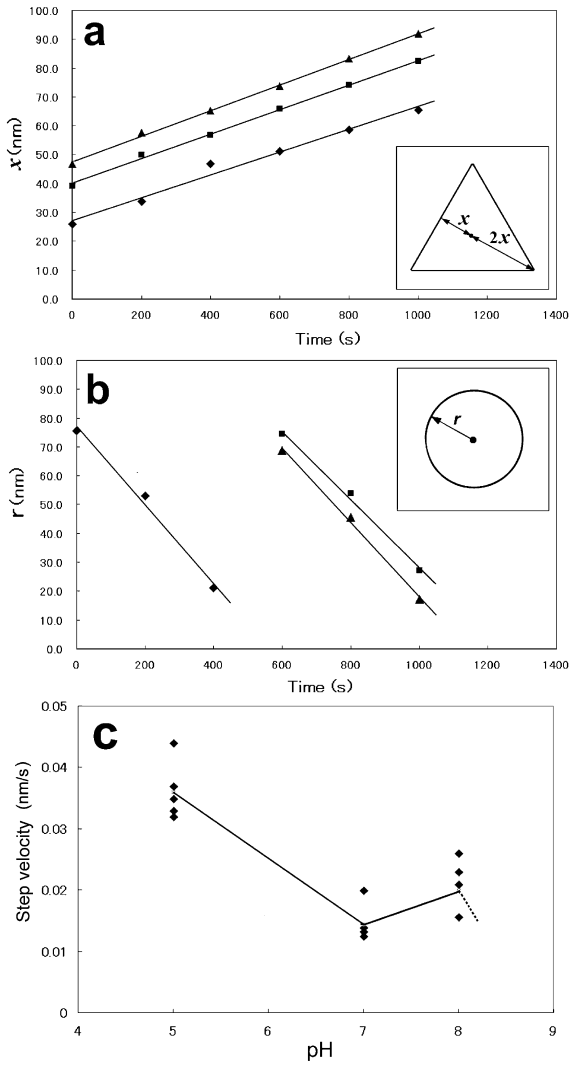


Figure 5. (a) The size of the triangular etch pits in Figure 1a as a function of time. The vertical axis is the distance from the center of the triangle to the side (x), which is calculated from the area of the triangle measured from AFM images. The three regression lines represent the different pits and the slopes of these lines correspond to the step velocity. (b) The sizes of the stranded terraces in Figure 1a with time. The vertical axis represents the radius of the circle with the same area as the terrace. (c) pH dependence of the step velocity around the triangular etch pits. The plots at pH 7 represent the result using de-ionized water.

First, the pH of the solutions may have changed from their initial values during dissolution. If we assume the dissolution rate of the brucite and the surface area of the specimen to be 1.0×10^{-8} mol m^{-2} s^{-1} and 1.0×10^{-5} m^2, respectively, then the dissolved brucite after several thousand seconds (Figure 5) is ~10^{-10} mol. This amount corresponds to the concentration of OH^- in the fluid cell (0.5 cm^3) of ~10^{-7} mol/L. Consequently, the pH of the de-ionized water must have increased (+1 pH) during the experiment. However, we would not expect the pH of the solutions initially at pH 5 and 8 to change considerably by the addition of this amount of OH^-.

The effect of ligands used for the solutions may be significant also. Recently, Pokrovsky *et al*. (2005) reported that the dissolution rate of brucite is affected by the type of ligands present in solutions. For instance, a high concentration (10^{-2} mol/L) of $H_2PO_4^-$ promotes the dissolution rate of brucite by two orders of magnitude at near-neutral pH values (Pokrovsky *et al*., 2005). Phthalic acid and tetraboric acid were used here for acidic and basic solutions, respectively, both of which were not examined by Pokrovsky *et al*. (2005). It is possible that the dissolution at pH 4 (Figure 3) and pH 9.2 (dissolution was not observed) were influenced by these ligands. However, the dissolution feature and step velocity in the other solutions at near-neutral pH were approximately similar to those in de-ionized water only, suggesting that the effect of the ligands is small for these conditions. Consequently, it is likely that the change of the solution composition and ligands did not seriously affect the dissolution rate at near-neutral pH.

Next, the step density used for the calculation (Figure 1) may not represent an 'average' step density of the brucite surface; the step density is a function of the etch pit density. Etch pit density, which must be correlated to the defect density in the crystal, is probably dependent on the specimen. Moreover, the contribution of the side surfaces of the crystal to the dissolution rate must also be considered because the step density on the side surfaces is very high (*e.g*. Rufe and Hochella, 1999). For a side surface being perpendicular to the basal surface, the density of the 'edge' of the layer is 2.1 nm^{-1}, which is 250 times greater than the step density in Figure 1. However, Jordan and Rammensee (1996) reported that the step velocity of brucite decreases considerably if the step density exceeds 0.1 nm^{-1}. This result is related to the increase of the probability that the species dissolved from a step and migrating on a terrace are trapped at neighboring steps before entering the solution. These trapping species can occur at the side surfaces and their contribution to the dissolution rate may be less than expected from their high step density. It is also difficult to estimate the ratio of the basal and side areas, which depends on crystal shape and microcleavage. Thus, a large discrepancy in the estimated dissolution rates may result, perhaps as much as one or two orders of magnitude between the dissolution rates derived from the AFM and bulk experiments, as reported by Shiraki *et al*. (2000) and Arvidson *et al*. (2003).

CONCLUSIONS

We have described the dissolution behavior of brucite by using AFM. The dissolution process at the atomic scale depends primarily on its crystallography. A future project will be to compare the results obtained with

https://doi.org/10.1346/CCMN.2006.0540506 Published online by Cambridge University Press

those from computer simulations (Lasaga and Luttge, 2003). We have also determined the step (retreat) velocity at a low step density and at near-neutral pH, which is an 'intrinsic' property of brucite. The dissolution rate of layer minerals is a product of step velocity and step density, and probably the combination of the results from AFM and bulk dissolution experiments are required to give a comprehensive understanding of the dissolution for these minerals.

ACKNOWLEDGMENTS

We thank Michiaki Bunno (Geological Museum, AIST, Japan) for donating the brucite specimen. We are grateful to Associate Editor Randall T. Cygan and two anonymous reviewers for their valuable comments. We also thank Steve Guggenheim for improving the English. This work was partly supported by a Grant-in-Aid No. 17340160 [Section (B)] by the Japan Society for the Promotion of Science (JSPS).

REFERENCES

Arvidson, R.S., Ertan, I.E., Amonette, J.E. and Luttge, A. (2003) Variation in calcite dissolution rates: A fundamental problem? *Geochimica et Cosmochimica Acta*, **67**, 1623–1634.

Binning, G., Quate, C.F. and Gerber, Ch. (1986) Atomic Force Microscope. *Physical Review Letters*, **56**, 930–933.

Bosbach, D. and Rammensee, W. (1994) In situ investigation of growth and dissolution on the (010) surface of sypsum by Scanning Force Microscopy. *Geochimica et Cosmochimica Acta*, **58**, 843–849.

Dove, P.M. and Platt, F.M. (1996) Compatible real-time rates of mineral dissolution by Atomic Force microscopy (AFM). *Chemical Geology*, **127**, 331–338.

Heaton, J.S. and Engstrom, R.C. (1994) *In situ* atomic force microscopy study of the differential dissolution of fayalite and magnetite. *Environmental Science and Technology*, **28**, 1747–1754.

Jordan, G. and Rammensee, W. (1996) Dissolution rates and activation energy for dissolution of brucite (001): A new method based on the microtopography of crystal surfaces. *Geochimica et Cosmochimica Acta*, **60**, 5055–5062.

Jordan, G., Higgins, S.R. and Eggleston, C.M. (1999) Dissolution of the periclase (001) surface: A scanning force microscope study. *American Mineralogist*, **84**, 144–151.

Kogure, T. (2002) Identification of polytypic groups in hydrous phyllosilicates using electron back-scattering patterns. *American Mineralogist*, **87**, 1678–1685.

Lasaga, A.C. and Luttge, A. (2003) A model for crystal dissolution. *European Journal of Mineralogy*, **15**, 603–615.

Peskleway, C.D., Henderson, G.S. and Wicks, F.J. (2003) Dissolution of gibbsite: Direct observations using fluid cell atomic force microscopy. *American Mineralogist*, **88**, 18–26.

Pokrovsky, O.S. and Schott, J. (2004) Experimental study of brucite dissolution and precipitation in aqueous solutions: Surface speciation and chemical affinity control. *Geochimica et Cosmochimica Acta*, **68**, 31–45.

Pokrovsky, O.S., Schott, J. and Castillo, A. (2005) Kinetics of brucite dissolution at 25ºC in the presence of organic and inorganic ligands and divalent metals. *Geochimica et Cosmochimica Acta*, **69**, 905–918.

Rufe, E. and Hochella, M.F. (1999) Quantitative assessment of reactive surface area of phlogopite during acid dissolution. *Science*, **285**, 874–876.

Shiraki, R., Rock, P. and Casey, W.H. (2000) Dissolution kinetics of calcite in 0.1 M NaCl solution at room temperature: An atomic force microscope (AFM) study. *Aquatic Geochemistry*, **6**, 87–108.

Vermilyea, D.A. (1969) The dissolution of MgO and $Mg(OH)_2$ in aqueous solutions. *Journal of Electrochemical Society*, **116**, 1179–1183.

White, A.F. and Brantley, S.L. (1995) *Chemical Weathering Rates of Silicate Minerals*. Mineralogical Society of America, Washington, D.C.

(*Received 14 March 2005; revised 26 April 2006; Ms. 1026; A.E. Randall T. Cygan*)

https://doi.org/10.1346/CCMN.2006.0540506 Published online by Cambridge University Press